Manuscript

Title:

HCS-3D*X*, a next-generation AI-driven automated 3D high-content screening system.

Authors:

Akos Diosdi [1,2,3,*], Timea Toth [1,3], Istvan Grexa [1], Bálint Schrettner [1], Nora Hapek [1], Ferenc Kovacs [2], Andras Kriston [2], Maria Harmati [1,4], Krisztina Buzas [1,4], Francesco Pampaloni [5], Filippo Piccinini [6,7], Peter Horvath [1,2,8,9].

Affiliations:

[1] Synthetic and Systems Biology Unit, HUN-REN Biological Research Centre (HUN-REN BRC), Szeged, Hungary.
[2] Single-Cell Technologies Ltd, Szeged, Hungary.
[3] Doctoral School of Biology, University of Szeged, Szeged, Hungary.
[4] Department of Immunology, University of Szeged, Szeged, Hungary.
[5] Buchmann Inst. for Molecular Life Sciences, Goethe-Universität Frankfurt am Main, Frankfurt am Main, Germany.
[6] IRCCS Istituto Romagnolo per lo Studio dei Tumori (IRST) “Dino Amadori”, Meldola (FC), Italy.
[7] Department of Medical and Surgical Sciences (DIMEC), University of Bologna, Bologna, Italy.
[8] Institute of AI for Health, Helmholtz Zentrum München, Neuherberg, Germany.
[9] Institute for Molecular Medicine Finland, University of Helsinki, Helsinki, Finland.
* Corresponding author: horvath.peter@brc.hu

Abstract:

Multicellular 3D biological models, the so-called “-oids”, are the pivot key for the new generation of high-content screening (HCS) of drug analysis, cancer research, and regenerative medicine. However, the standardisation of 3D cell culture generation, handling, imaging, and data analysis remains a challenge and lacks convincing applications. In this work, we propose HCS-3D*X*, a next-generation system revolutionising HCS research in 3D imaging and evaluation. HCS-3D*X* is based on three main components: an automated Artificial Intelligence (AI)-driven micromanipulator for oid selection, an engineered HCS foil multiwell plate for optimised imaging, and an image-based software for single-cell data analysis. The developed

system was validated through different experiments with 3D tumour models, including tumour-stroma co-cultures. The results prove that the resolution achievable with HCS-3D*X* enables us to overcome the limitations of current systems and reliably perform 3D high-content screening (HCS) at the single-cell level.

Keywords: 3D cell cultures, multicellular 3D tumour models, Micromanipulation, High-content screening, Artificial intelligence, Automated light-sheet microscopy, 3D single-cell analysis.

Introduction

For many years, two-dimensional (2D) monolayer cell cultures have been extensively used as model systems to assess drug effects. However, it has been shown that 2D cell cultures do not accurately capture the physiological characteristics of tissues and the tumour microenvironment [1]. Three-dimensional (3D) cell cultures are gaining more attention as a relevant model system for drug testing [2]. Especially, the so-called "-oids" (*e.g*. spheroids, organoids, tumouroids, and assembloids) are broadly tested and proven to mimic *in vivo* conditions and maintain tissue structure which makes them highly relevant in numerous biological research areas, including drug discovery, tumour biology, and immunotherapy [3, 4, 5].

Since 2010, the constantly increasing attention on 3D cell cultures resulted in almost 30,000 articles and almost 350,000 publications discussing high-content systems. However, only 1% of these publications represent high-content screening (HCS) works based on imaging systems and little over 70 contributions refer to HCS imaging of 3D-oids (**Supplementary Table 1**). These small numbers show that there are challenges in developing 3D HCS platforms, including -oid generation, handling, imaging, and analysis.

At the level of 3D-oid generation, there are concerns about: (*a*) morphological variability [6], (*b*) penetration properties of compounds and stainings [7], (*c*) inner distribution and biological characteristics of the cells [8]. Many researchers are working on standardising generation protocols [9], but due to the nature of the 3D models, high variability is still expected especially when hundreds of 3D-oids are imaged. To handle 3D-oids and ensure experimental reproducibility, Artificial Intelligence (AI)-driven systems for manipulating and selecting similar aggregates are proposed [10, 11, 12]. For instance, AI-driven micromanipulators combining morphological pre-selection with automated pipetting systems, reduce time and ensure reliability when transferring spheroids to the imaging plates [13]. For complex drug screenings, single-cell phenotyping is needed

and this requires imaging at the highest resolution [14]. Light-sheet fluorescence microscopy (LSFM) is able to visualise large samples at the cellular level with high imaging penetration, minimal phototoxicity and photobleaching [15, 16]. To date, the available LSFM HCS plates for 3D-oids have different drawbacks (*e.g*. different sample preparation, light penetration, imaging time). In addition, the amount of generated data is typically vast and heterogeneous. The analysis results in a time-consuming and computationally demanding procedure, requiring automation. Several pipelines and tools have been introduced for the analysis of 3D data, but no standard has been defined for the quantitative tasks, like segmentation, classification, and feature extraction [17, 18, 19].

In this work, we propose HCS-3D*X*, a customisable 3D imaging and analysis HCS system for 3D-oids at a single-cell level (**Fig.1a**). It includes (*I*) selection and transferring of morphologically homogeneous 3D spheroids by the self-developed *SpheroidPicker* (**Fig.1b**); (*II*) single-cell LSFM imaging using a custom Fluorinated Ethylene Propylene (FEP) foil multiwell plate (**Fig.1c**); (*III*) 3D data analysis with *Biology Imaging Analysis Software* (*BIAS*, Single-Cell Technologies, Szeged, Hungary) [20] (**Fig.1d**) . Different types of experiments were performed to show how HCS-3D*X* can be reliably used for single-cell 3D HCS. First, morphological analysis of tumour spheroids under different conditions was executed to define the best setup for 3D-oids selection using the *SpheroidPicker*, an AI-guided, 3D cell culture delivery system [13]. Then, the accuracy of 2D features at multiple levels was validated using monoculture spheroids. Before extending the feature analysis to 3D, a specific test was performed to quantify screening performance and image quality when using the designed HCS foil multiwell plate. Finally, the effectiveness of the HCS-3D*X* system was proven on co-culture tumour models via quantitative evaluation of tissue composition at a single-cell resolution.

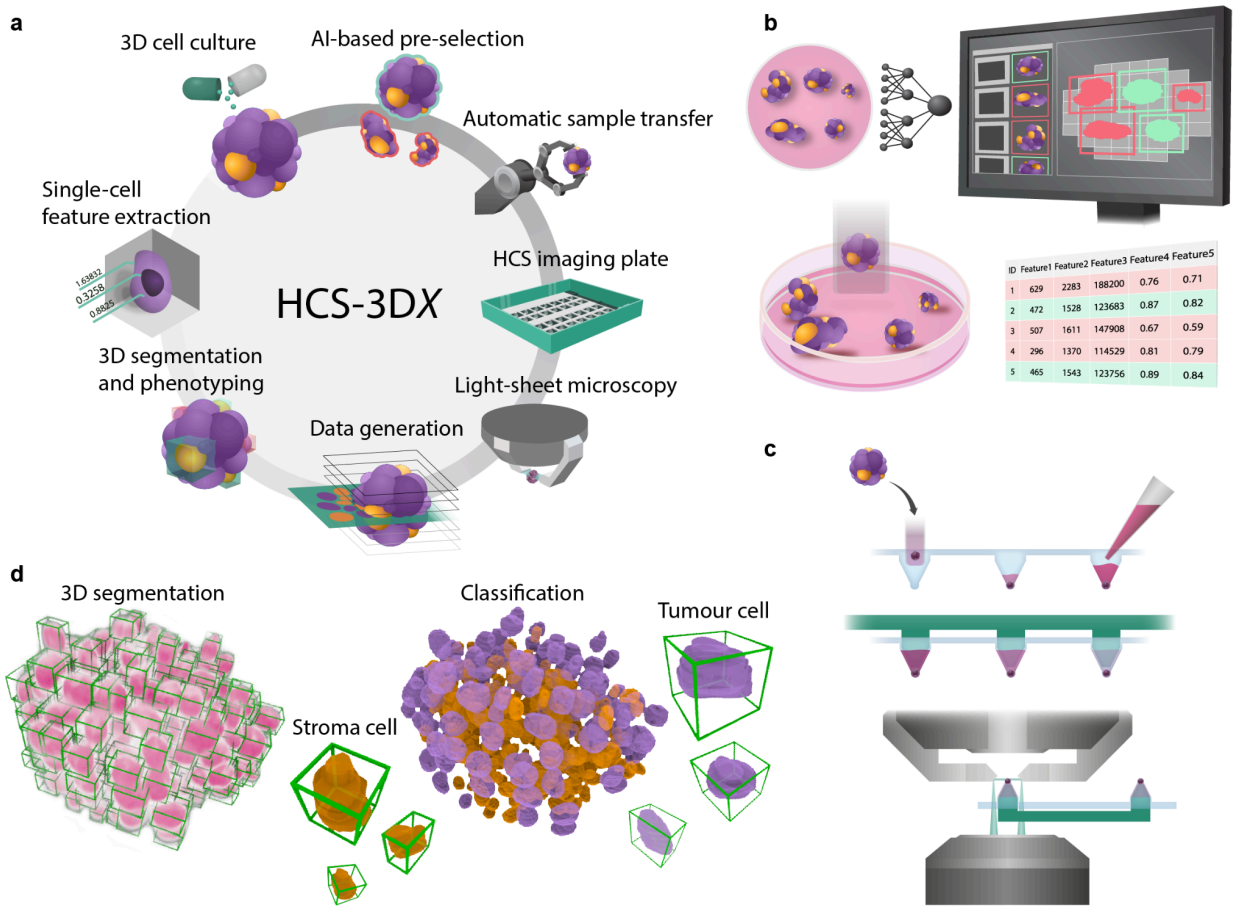

ID	Feature1	Feature2	Feature3	Feature4	Feature5
1	629	2283	188200	0.76	0.71
2	472	1528	123683	0.87	0.82
3	507	1611	147908	0.67	0.59
4	296	1370	114529	0.81	0.79
5	465	1543	123756	0.89	0.84

Fig.1 HCS-3D*X*, an AI-driven 3D imaging and analysis HCS system for 3D-oids at a single-cell level. (**a**) HCS-3D*X* includes 8 essential steps: (*I*) 3D cell culture generation, (*II*) AI-driven 2D feature analysis and object selection, (*III*) automated sample transferring from the source culture vessel, (*IV*) transfer to a custom-developed HCS imaging plate, (*V*) LSFM screening, (*VI*) generation of massive 3D image datasets, (*VII*) image analysis with *BIAS* (*VIII*) feature extraction and single-cell classification. (**b**) Step *II-IV* - working principle of the *SpheroidPicker*, an AI-guided, 3D cell culture delivery system using a light microscope for 2D morphology-based spheroid screening and analysis, enabling semi- or fully automated transfer of selected spheroids with predefined morphology. (**c**) Step *IV* - selected spheroids are transferred to the HCS foil multiwell plate compatible with LSFM to obtain single-cell resolution in 3D. (**d**) Step VII - a representative image of a nuclei-labelled spheroid analysed and visualised by BIAS, with single cells indicated by green bounding boxes [21].

The developed HCS-3D*X* platform overcomes many limitations of the current analysis of 3D-oids. HCS-3D*X* comprises all the steps required to evaluate 3D cell cultures from the beginning to the end at a single-cell level by enabling reliable, fast and automatic high-content imaging of multiple 3D-oids with a high penetration depth. Consequently, the proposed concept is advantageous for a wide range of research purposes, including industrial drug screening, personalised medicine, or basic research.

Results:

2D features variability.

In the first experiment, a comparative study was executed for the pre-selection of spheroids generated under the same conditions. To verify the ideal screening parameters in 2D, brightfield images obtained by various objectives have been compared by obtaining radiomic features of co-culture spheroids. The same spheroids were imaged at different magnifications (**Supplementary Table 2**). Fifty spheroids were imaged with 2.5x, 5x, 10x, and 20x objectives resulting in 200 images. The images were manually annotated and 2D morphological features were extracted using *BIAS* and *ReViSP* (a specific tool for estimating the volume of spheroids using a single 2D brightfield image [22]). On average, for all the extracted features (*Diameter*, *Perimeter*, *Area*, *Volumetry*, *Circularity*, *Sphericity*, and *Convexity*), the relative differences between different magnifications (considering 20x as a reference) were less than 5%, except for *Volumetry* that reached ~7% (**Fig.2a** and **Supplementary Table 3**). *Perimeter*, *Sphericity*, *Circularity*, and *Convexity* showed significant differences between the 2.5x and the 5x/10x objectives since the lower image resolution resulted in a less accurate representation. To provide the most accurate comparison, the 20x objective was used as a reference for all further experiments.

Spheroid models variability.

In order to measure model heterogeneity, mono- and co-culture spheroids generated by 3 experts with extensive daily experience in 3D cell cultures have been compared. The experts repeated exactly the same experiments 3 times (**Fig.2b-d**). Overall 426 spheroids were generated, 223 monoculture and 203 co-cultures. For the monoculture spheroids, each expert counted and manually plated 100 HeLa Kyoto cells for each well. In the case of co-cultures, each spheroid contained 40 HeLa Kyoto cells and 160 MRC-5 cells. Each spheroid was manually annotated to extract the 2D features. Although all the experts used the same equipment within the same environment and followed exactly the same instructions, the comparison showed a great heterogeneity regarding spheroids' size and shape (**Fig.2c**). By evaluating the 2D features of the monoculture spheroids, *Expert 1* generated significantly bigger spheroids (**Fig.2b** and **d**). Although the range of *Volumetry* is wide, *Sphericity* values were independent of the spheroids' size and there were no significant differences between the experts and batches. Differences were visible between experts and in between batches when generating the spheroids with two different cell lines (**Fig.2d**). Compared to

monocultures, the spheroids produced using two cell lines had twice as many cells and, on average, smaller *Volumetry*, indicating more compact spheroids.

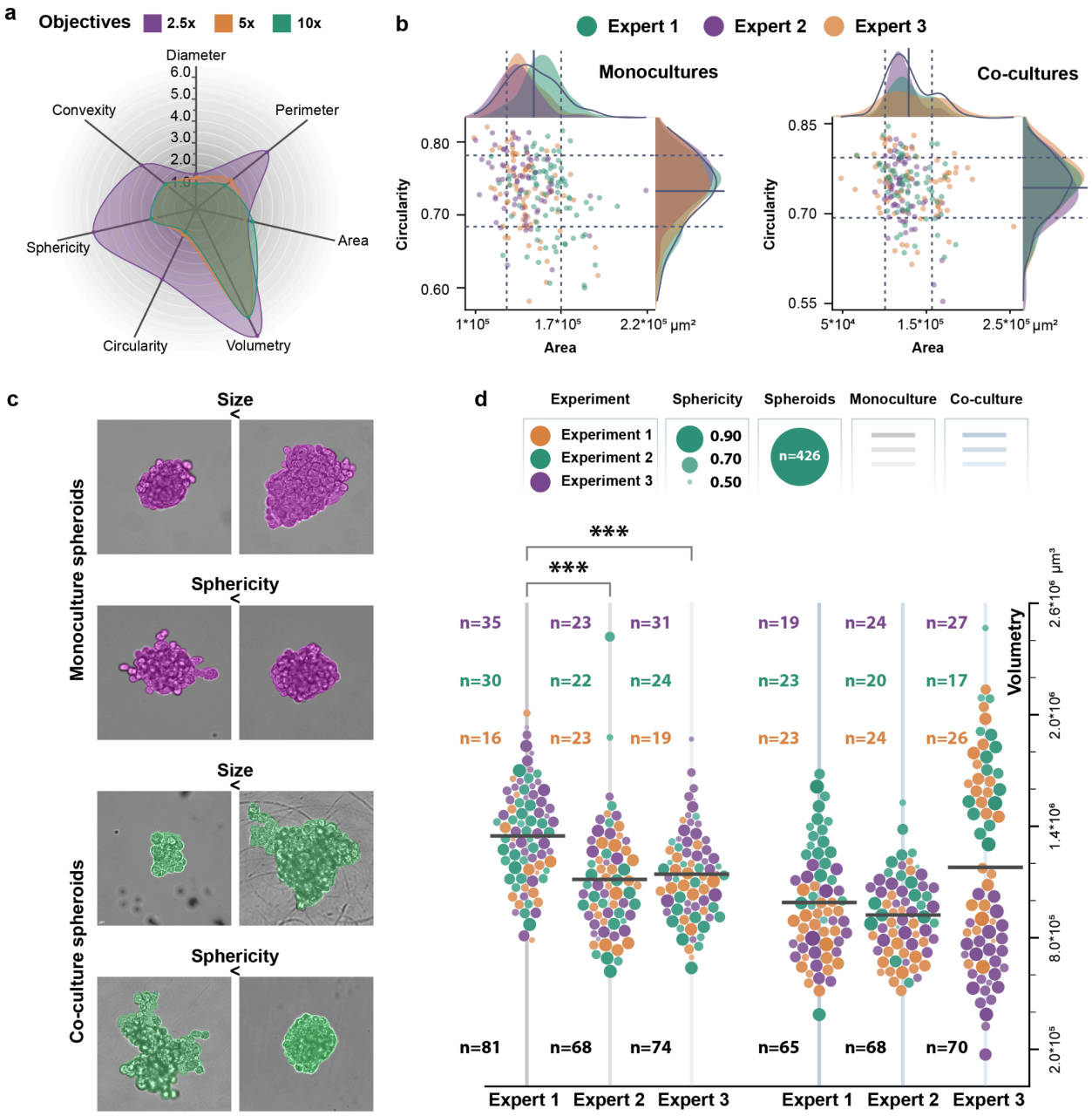

Fig.2 (**a**) The spider plot visualises the relative differences of features acquired by annotating the same spheroids, imaged by 4 objectives with different magnifications. Each objective was compared to the annotations that were executed on the images of the 20x objective. After manual annotation, features such as *Diameter*, *Perimeter*, *Area*, *Volumetry*, *Circularity*, *Sphericity*, and *Convexity* were displayed. The 2.5x objective resulted in the fastest imaging including finding and focusing, however, it showed the least accurate feature extraction. Both 5x and 10x objectives are ideal for imaging spheroids since they increase the imaging speed slightly while providing relatively accurate values. 20x objective is the most accurate but it requires more time to find and focus the spheroid. n=50 (**b**) Distribution of monoculture and

co-culture spheroids based on the *Area* and *Circularity* features. Each circle represents a spheroid, and each colour corresponds to a different expert (green - *Expert 1*, purple - *Expert 2*, and orange - *Expert 3*). The central lines display the average value for all the samples whilst the dashed lines display the plus and minus one standard deviation. (**c**) Representative images of the 2D annotated dataset including monoculture (purple) and co-culture (green) spheroids with the smallest and largest volumes and least and greatest sphericity values. (**d**) Beeswarm plot of the monoculture (grey) and co-culture (light blue) spheroids divided by experts (vertical distribution) and experiments (orange - *Experiment 1*, green - *Experiment 2*, purple - *Experiment 3*), indicating the volumetry and sphericity of each sample. Overall 426 spheroids were screened. Each circle represents a spheroid on a volumetry axis showing the sphericity values by the size and intensity (bigger and more intensive circles represent the most spherical spheroids). The number of spheroids evaluated in each batch is displayed, with different colours representing individual experiments and black indicating the total count. *$p \leq 0.05$; **$p \leq 0.01$; ***$p \leq 0.001$.

HCS imaging plate for LSFM

An HCS plate with predefined positions for the samples was designed to allow fast and automatic multiple object screenings (**Fig.3** and **Supplementary Note 1**). The plate was developed and tested on the Leica TCS SP8 DLS upright LSFM (Germany). To validate the image quality and measure the screening time, T-47D spheroids were generated with a diameter under 200 µm. 2 different groups of 5 spheroids were defined: as recommended by Leica, the first 5 were embedded into agarose and placed into individual Petri dishes; the other 5 spheroids were placed into the HCS plate (**Supplementary Fig.2**). The difference between the groups was minimal and not noticeable to the naked eye (**Supplementary Fig.2a**). Therefore, the quality of the images was measured by the intensity variance metric that can characterise the general blurriness of an image qualitatively [23]. Considering the average values, no significant differences were observed, suggesting similar image quality (**Supplementary Fig.2b**). Although the spheroids screened with the HCS plate showed slightly better scores, this phenomenon can be explained by size and morphology differences of the randomly selected spheroids. This same image quality was already achieved [24], but further analyses were performed to prove the effectiveness of the HCS plate. To measure the average screening time, 10 spheroids were separated into Petri dishes and embedded into agarose, while the other 10 spheroids were placed into the HCS plate. Comparing the total screening time, the HCS plate performed twice as fast (~50 min) meanwhile the screening time in the Petri dishes took approximately 102±9 min (**Supplementary Fig.2c**). The largest differences were observed during the sample preparation processes: manually plating the spheroids into the plate took 14±2 min, while embedding the spheroids into agarose took approximately 37±5 min. Another significant difference appeared during the calibration process, where replacing and calibrating each spheroid took approximately 26±4 min. This does not apply to the plate since all 10 spheroids were separated and placed into individual cuvettes. Other calibration and imaging processes took 30±3 min for both approaches. However, finding samples within

the plate is easier, as all positions are predefined and one calibration at the beginning is sufficient. Overall, the custom-developed HCS plate is easy to use, it reduces the imaging time and ensures the same image quality compared to the dishes recommended by the manufacturer.

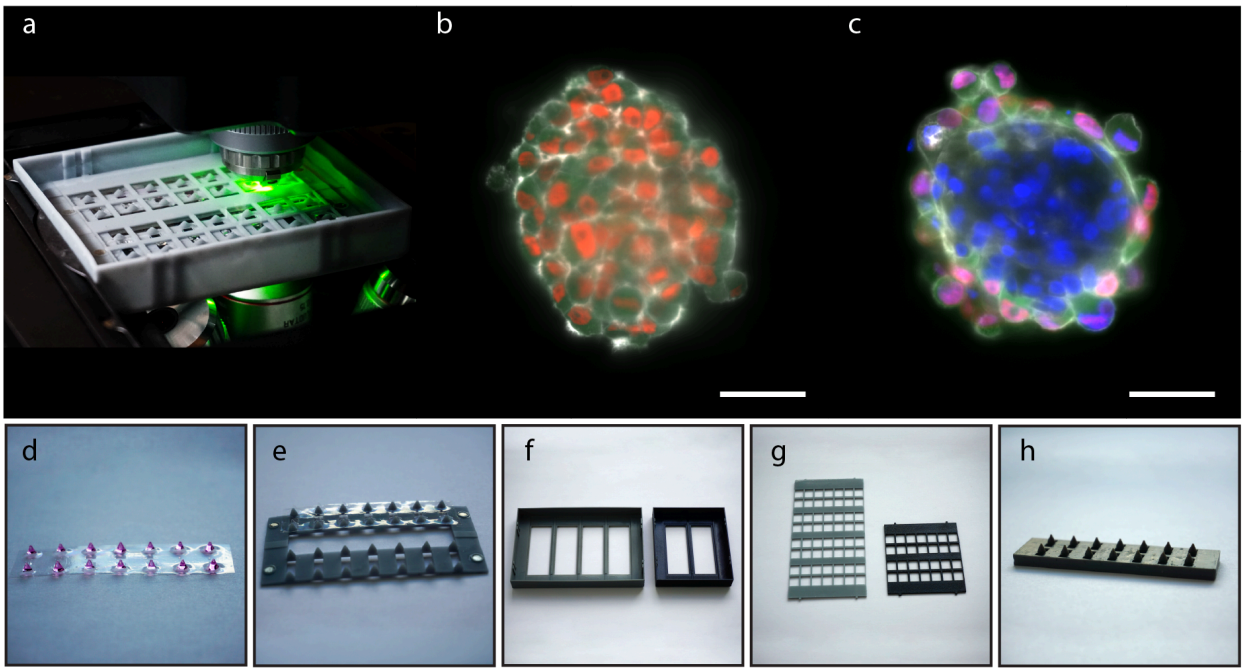

Fig.3 Concepts of the HCS plate. (**a**) Illustration of the HCS plate. (**b**) A representative image of a monoculture spheroid composed of HeLa Kyoto cells (green - EGFP-alpha-tubulin; red - H2B-mCherry; grey - actin). The scale bar represents 50 µm. (**c**) A representative image of a co-culture spheroid comprising HeLa Kyoto and MRC-5 cell lines (blue - DAPI, green - EGFP-alpha-tubulin; red - H2B-mCherry; grey - actin). The scale bar represents 50 µm. (**d**) Vacuum-formed transparent FEP foil where each cuvette is suitable for one sample. For visualisation, each cuvette was filled with cell culture media. (**e**) The insert element that fits into the cuvettes of the foil. The insert element only secures the position of the samples at the bottom of the cuvettes. (**f**) The base of the plate is an additional component that provides volume for the detection solution and space inside the plate for the water immersion objectives. Two versions are available. (**g**) The grid element that fits into the base prevents the movement of the FEP foil after filling up with the detection solution. Two versions are available for each base (**h**) 3D printed heat-resistant mould element that was used to form the FEP foil.

3D single-cell analysis of spheroid models.

114 HeLa Kyoto/MRC-5 co-culture spheroids, randomly selected between those generated by the 3 experts in 3 batches, were 3D screened using the HCS foil multiwell plate. Then, they were analysed at a single-cell level through segmentation and classification using *BIAS*. Results on cell ratio showed that only 24% of the 114 spheroids predominantly consisted of HeLa Kyoto cells (hereafter called *HeLa Kyoto*

majority group), while 67% primarily contained MRC-5 cells (hereafter called *MRC-5 majority group*, **Fig.4a**). Only 10 spheroids showed equal numbers of the 2 cell lines (hereafter called *Equal group*). By dividing spheroids based on their class (*HeLa Kyoto majority*, *Equal*, and *MRC-5 majority group*), an increased total cell number was identified for the *MRC-5 majority group* (**Fig.4b**). There were no significant differences in the cell ratio of spheroids generated by the experts. However, in some cases, more consistent spheroid formations were noted. For instance, Expert 1 and 2 in batch 2 consistently generated spheroids with more MRC-5 cells (**Fig.4c**).

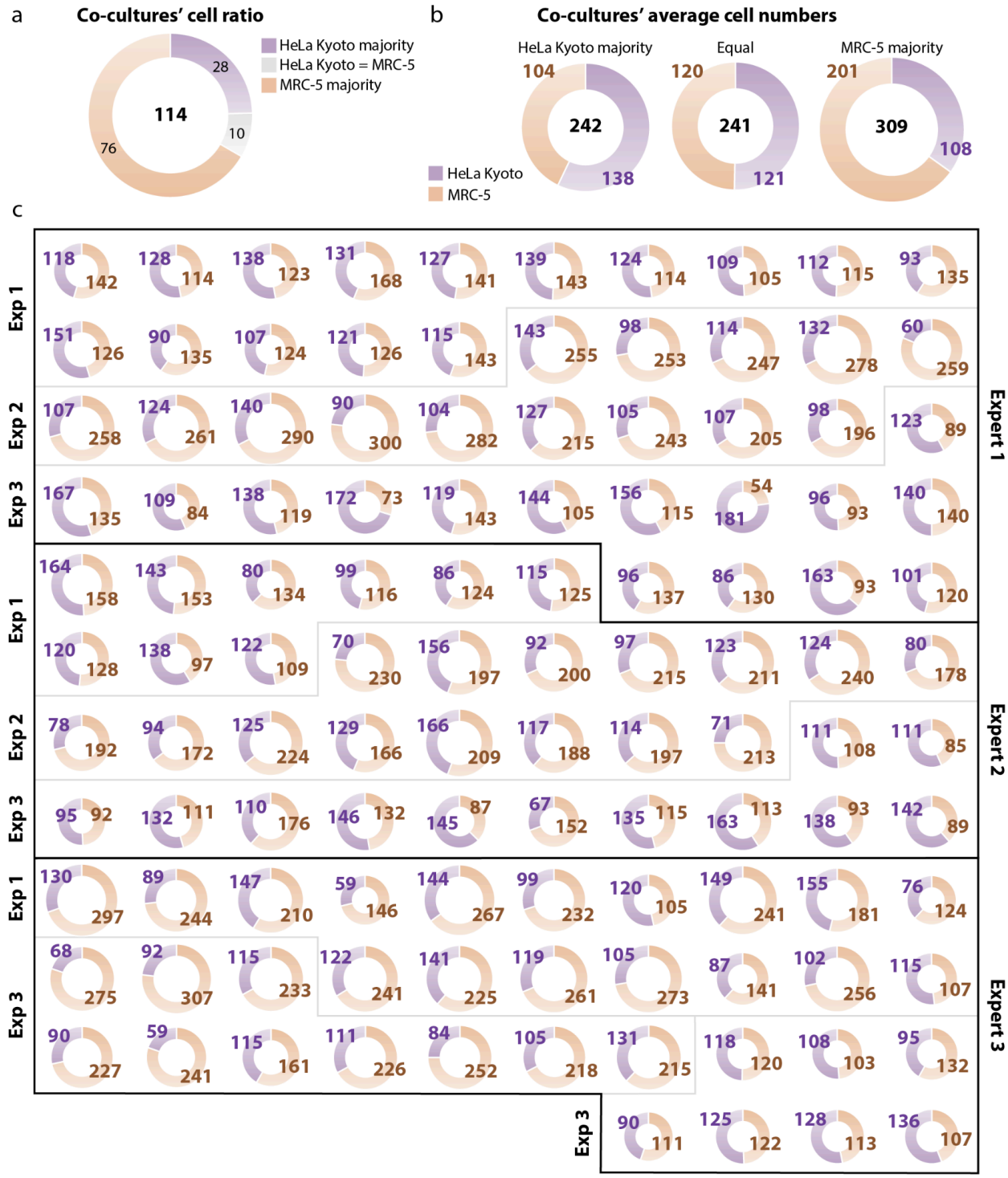

Fig.4 Single-cell analysis of co-culture spheroids. (**a**) Cell ratio for the 114 co-culture spheroids, showed 76 spheroids with MRC-5 cells in majority (orange), 28 spheroids with HeLa Kyoto majority (purple), and 10 spheroids with an equal number (grey). (**b**) The 114 spheroids were divided into 3 groups based on the cell type in majority (*i.e.* HeLa Kyoto majority, Equal, MRC-5 majority). The size of the doughnut charts and the numbers in their centre represent the average cell numbers for each group. The average number of cells for each class is displayed with dark orange for HeLa Kyoto and dark purple for

MRC-5. (**c**) Individual spheroids are displayed and separated by experts and experiments where the size of the doughnut chart refers to the total number of cells (also reported in coloured numbers); n=114.

Discussion

Analysing the literature of the last 10 years, it is evident that the number of works based on HCS quickly rose. Between 2010 and 2023 the number of publications reached over 305,000. Similarly, but lower of an order of magnitude, the number of works citing 3D-oids rapidly increased and today is around 4000 articles/year. However, the number of imaging-based works is significantly lower, 1% in the case of HCS and 5% in the case of 3D-oids. One possible explanation is the technological issues hinder the practical use of 3D HCS imaging platforms, primarily the light penetration that limits the acquirable single-cell signals and the lack of fully automated systems that require less human resources. After an in-depth methodological analysis of publications, 70 scientific articles were published over the past ten years providing insight into the challenges and discussing possible solutions, but none of them provided a practical reliable solution for performing single-cell 3D HCS.

In this work, we presented HCS-3D*X*, a customisable 3D imaging and analysing HCS system for 3D-oids at a single-cell level. This innovative system addresses several challenges associated with 3D HCS, including the pre-selection, handling, imaging, and analysis of 3D-oids. The main concept of this work concludes an HCS plate that was designed to separate and allow fast and automatic multiple object screenings within the same plate, where the position of the samples is predefined. The plate was developed and tested on an upright light-sheet microscope to achieve single-cell resolution in spheroids, however, any type of 3D cell culture can be screened. The compatibility with a multi-pipette or a pipetting robot reduces the time-consuming sample preparation and transfer processes. Furthermore, long-term live imaging of the specimen in the plate is optimal since the FEP foil allows gas exchange. By integrating AI-driven solutions and advanced imaging techniques such as LSFM, HCS-3D*X* enables precise, automated, and high-throughput analyses at a single-cell level. To test HCS-3D*X*, 3 different types of experiments, considering radiomic analysis of monoculture and co-culture spheroids were performed.

In the first experiment, several microscope settings were compared by extracting radiomic features of co-culture spheroids. The results proved that selecting spheroids for an HCS experiment is crucial in many aspects, but for many reasons, reproducibility is the most essential. Considering image-based features, certain 2D parameters are more important than others when pre-selection is an option. Most publications describe 3D samples using *Diameter*, *Perimeter*, *Area*, *Volumetry*, *Circularity*, *Sphericity*, and *Convexity*. Even though the average differences were less than 5% between the

objectives, significant differences were measured between the 2.5x, the 5x and 10x objectives. Among the tested features, we observed that only *Perimeter*, *Convexity*, *Sphericity*, and *Circularity* showed significant differences. The higher magnification images resulted in more precise contours that follow the edge of the objects accurately. Meanwhile, annotations on images taken with lower magnification objectives were less accurate. The differences between the annotations caused discrepancies for *Perimeter* and for all the features that rely on it (*e.g. Circularity, Sphericity*, and *Convexity*). In addition to the objective's physical parameters (such as magnification, numerical aperture, and spherical aberration), the lower image resolution and the accuracy of the annotator caused the general inconsistency between the objectives. Therefore, a 10x objective is recommended to have a fair compromise for general feature reliability if 20x is unavailable or has an excessively narrow field of view, even though the 2.5x or 5x objectives would not distort the entire analysis.

The heterogeneity of spheroids is influenced by the type of cell, the environment, and the formation method, making the generation of 3D cell cultures complex [9]. In the second experiment, 426 monoculture (223) and co-culture (203) spheroids were analysed in 2D to measure the variability of the models. 3 experts repeated the same experiments 3 times. Despite using identical equipment and working in the same environment, the comparison of the manual plating revealed great heterogeneity in spheroids' sizes and morphology. Considering different batches, an expert could make consistently bigger spheroids compared to others. Furthermore, significant differences were measured by comparing the performance of the various experts. By generating spheroids from a single cell line, we demonstrated that a higher number of replicates and a proper 2D feature quantification are recommended.

In the third experiment, we quantified screening performances and image quality reachable when using our custom-made 3D-printed HCS foil multiwell plate. It is noteworthy that while confocal microscopy is limited in penetration depth, LSFM offers greater performances with reduced phototoxicity and increased imaging speed. However, it often requires complicated and time-consuming sample preparation processes which significantly limits its potential and today there is no reliable HCS system for LSFM. In this work, using a Leica SP8 TCS DLS, we proved that the designed multiwell plate enables fast (reduces screening time by half) and automatic high penetration depth (we reached 250 µm for optically cleared spheroids [23, 24]) LSFM screenings of spheroids.

Increasing the complexity of the biological model introduces more bias into the experiment, potentially leading to incorrect conclusions. This complexity affects the classification of the two different cell types within the spheroids, making it difficult to

determine the exact ratio in the co-culture. Achieving single-cell resolution and applying 3D analysis (including segmentation, classification, and feature extraction) could provide a viable solution. 114 co-culture spheroids were analysed and compared at a cellular level. After counting the individual cells composing the spheroids, 3 groups were created (*HeLa Kyoto majority*, *Equal*, and *MRC-5 majority group*). The groups showed different cell ratios and unequal total cell numbers indicating the heterogeneity of the model. The total number of cells revealed that spheroids with more cells contained more MRC-5 than HeLa Kyoto. In this large-scale, single-cell analysis experiment, we demonstrated that complex models relying on interactions between various cell types result in high variety. However, the consistency of morphologically similar spheroids varies with the expert conducting the experiment as well. The size and structural differences of the co-culture models emphasise the need for a single-cell analysis pipeline to avoid incorrect data interpretations and false conclusions.

HCS-3D*X* comprises all the steps to evaluate 3D cell cultures from the beginning to the end at a single-cell level. Accordingly, it represents a substantial leap forward in 3D HCS, offering a comprehensive solution that bridges the gap between traditional 2D models and complex *in vivo* environments. Its application enhances the accuracy and efficiency of drug screening processes, supports personalised medicine approaches, and facilitates more detailed investigations into cellular behaviour within 3D structures. Concluding, the system's robustness and versatility make HCS-3D*X* a valuable tool for researchers and clinicians, paving the way for future innovations in biomedical research.

Materials and Methods

Cell lines

Spheroid monocultures were generated using the HeLa Kyoto EGFP-alpha-tubulin/H2B-mCherry cervical cancer cells (Cell Lines Service, Eppelheim, Germany). The maintenance of cell cultures was done under the manufacturer's instructions. Cells were maintained in a HeLa Kyoto medium consisting of DMEM (Lonza, Basel, Switzerland), 10% Fetal Bovine Serum (FBS, Euroclone, Milan, Italy), 2 mM L-glutamine (Lonza), 0.5 mg/ml G418 (Gibco, Montana, United States), and 0.5 µg/ml puromycin (Sigma, Kanagawa, Japan) was used. To generate uniform spheroids, 100 cells were seeded into each well in U-bottom cell-repellent 384-well plates (Greiner Bio-One, Kremsmünster, Austria) for 48 h at 37 °C and 5% CO_2. After 48 h, spheroids were collected and then washed 3 times with Dulbecco's Phosphate Buffered Saline (DPBS), and fixed with 4% Paraformaldehyde (PFA) for 60 min. Spheroids were washed with DPBS 3 times, and stored at 4°C in DPBS until imaging. Before imaging, spheroids were incubated in 0.1% Triton X-100 overnight at room temperature and

washed 3 times with DPBS. For actin labelling, spheroids were stained with 1:200 Flash Phalloidin NIR 647 (Biolegend, San Diego, California) for 60 min. Before the imaging, spheroids were washed with DPBS 3 times.

Co-culture spheroids were generated using the same HeLa Kyoto cells and MRC-5 fibroblasts (American Type Culture Collection - ATCC). The manufacturer's instructions were followed for the maintenance of the cell cultures. To generate spheroids, a co-culture medium consisting of DMEM, 10% FBS (Euroclone), 1% L-glutamine (2 mM), and 1% Penicillin-Streptomycin-Amphotericin B mixture (all from Lonza) was used. 40 HeLa Kyoto cells were seeded into each well in U-bottom cell-repellent 384-well plates at 37 °C and 5% CO_2. After 24 h of incubation, 160 MRC-5 cells per well were added onto the HeLa Kyoto cells and the co-cultures were incubated for one more day. After 24 h, the co-culture spheroids were collected from each well and washed 3 times with DPBS. 4% PFA was used for 60 min to fix the samples, then washed again with DPBS 3 times and stored at 4°C in DPBS until imaging. Before imaging, spheroids were incubated in 0.1% Triton X-100 and 1 µg/ml DAPI overnight at room temperature and washed 3 times with DPBS. Spheroids were stained with 1:200 Flash Phalloidin NIR 647 for 60 min. In the end, spheroids were washed with DPBS 3 times.

HCS foil multiwell plate

In this work, a customisable 3D imaging multiwell plate is designed for the screening of 3D-oids at a single-cell level. It includes: (*I*) a 3D printed base element that retains the detection fluid; (*II*) a FEP foil for separating the position of the samples; (*III*) an insert element to secure the samples' position within the foil; and (*IV*) a 3D printed grid element to fix the FEP foil position (**Fig.3**). This designed plate is suitable for examining a large number of samples with a LSFM, containing in each cuvette a single sample. The main parts of the plate are briefly discussed in the following sections, whilst detailed information about the dimensions and assembly are available in Supplementary Note 1.

FEP foils are fully transparent, with a refractive index of 1.341-1.347. FEP is chemically inert and resistant to organic solvents, acids, and bases, just like the majority of fluorocarbon plastics. Additionally, the material satisfies FDA (21CFR.177.1550) and EU (2002/72/EC) requirements [15]. FEP-films (Holscot Europe, Netherlands) with a 50 µm thickness were cut into 15x15 cm pieces and cleaned with 70% alcohol. Each foil was placed and clamped into the frame of a JT-18 vacuum-forming machine (Yuyao Jintai Machine Company, China). To get small and uniform shapes, the heater needs to raise the temperature to a level near the glass transition temperature of the FEP-foil (260–280°C). Once the heater reaches the desired temperature, the positive mould is quickly placed onto the vacuum-forming machine, and the foil is quickly pressed onto the mould whilst the vacuum suction is switched on. The FEP foil that has been

extruded is then carefully taken out of the mould and cleaned with an isopropyl alcohol bath for 5 min to remove the excess resin components.

Using *Blender 3.0*, positive moulds for the spikes were created. Each mould was designed to shape the FEP foil in order to fit perfectly into the base element. For printing, the 3D models were exported to a stereolithographic file format (.stl) and then imported into *PrusaSlicer v 2.6.x* (Prusa Research, Czech Republic). Each heat-resistant mould was printed with the Prusa SL1 printer, a stereolithography (SLA) resin-based 3D printer that forms objects layer by layer using a liquid resin that is UV-cured. This printer provides high-resolution printing capabilities enabling the production of intricate and detailed objects with smooth surfaces. The mechanical and thermal characteristics of heat-resistant resin enable it to endure the vacuum-forming process. The positive moulds were UV-cured and washed with isopropanol to remove excess resin from the surface. Then the moulds were examined under a stereomicroscope and cleaned by submerging them in an ultrasonic bath before being used.

The base components of the plates were printed with the Prusa i3 MK3S+ 3D printer with PETG (3DP-PETG1.75-01-BK; Gembird, Shenzhen, China) in two different sizes. The model was sliced with *PrusaSlicer*. 3D printed with default Prusa PETG filament profile and with “0.2 Quality print settings” using a 0.4 nozzle. The bigger version is 85 mm / 127 mm / 15.4 mm (average size of a 96-well plate) which is suitable for screening 56 samples, while the smaller version 85 mm / 73.8 mm / 15.4 mm was designed only for 28 samples. To create a waterproof base for the samples, the 24 mm / 64 mm cover glasses (Menzel Gläser, Germany) were secured with silicon grease (ThermoFisher, USA) to the bottom of the bases. The cover glass provides a transparent bottom for any inverted microscopy setup while allowing the freedom of using dipping objectives.

A grid element was 3D printed using a Prusa i3 MK3S+ printer with PETG to prevent the samples from shifting after being filled with mounting media. The grid element can be slid into predefined spaces, securing the foil to the bottom of the plate.

Microscopes

For the brightfield images, the fixed monoculture and co-culture spheroids were placed into a cell culture dish 35/10 mm with a glass bottom (627965, Cellview, Austria) in PBS. Brightfield images were taken with the Leica SP8 TCS using 4 different objectives: 2.5x/0.07, 5x/0.15, 10x/0.32, and 20x/0.4 (**Supplementary Table 2**).

The HCS foil multiwell plate was validated on the Leica TCS SP8 Digital LightSheet (DLS) microscope, exploiting a standard 96-well plate insert. A 25x/0.95 detection

objective with a mounted 2.5 mm mirror device was used to capture fluorescence DLS images, illuminated by the 2.5x/0.07 objective. Images with a resolution of 2048×2048 pixels and a pixel size of 0.144 µm were captured with the sCMOS DFC9000 Leica camera. A 2 µm gap distance between the images was used in each z-stack. dH_2O mounting medium was used for every spheroid. 3 different tests were performed changing laser and laser intensity (**Supplementary Fig.2** and **Fig.4**). Firstly, a laser with a wavelength of 638 nm and an exposure time of 200 ms with 20% laser intensity (maximum laser intensity 350 mW) was used. Then, laser intensity was manually adjusted for each channel (*i.e*. 405, 488, 552, and 638 nm wavelength).

Image analysis

Brightfield images were annotated using the *AnaSP* software [25] to obtain binary masks and *Volumetry* features. Original brightfield images and corresponding masks were imported into *BIAS* and 2D features were exported [20]. Image quality was evaluated using intensity variance, a metric implemented in *Spheroid Quality Measurement* (SQM), an open-source *ImageJ*/*Fiji* plugin [23]. All the 3D fluorescent image stacks were directly analysed in *BIAS* using algorithms based on *StarDist* [26] for segmentation and multilayer perceptron (MLP) for classification.

Statistical analysis

Statistical analyses were conducted using GraphPad Prism 8 software. The Kolmogorov-Smirnov test was applied to assess normal distribution. For analysing the results of the 2D features, the non-parametric Kruskal-Wallis test followed by Dunn's multiple comparisons was used. The significance level was set at $\alpha = 0.05$ with a 95% confidence interval, and p-values were adjusted for multiple comparisons.

References:

[1] Duval, K., Grover, H., Han, L. H., Mou, Y., Pegoraro, A. F., Fredberg, J., & Chen, Z. Modeling physiological events in 2D vs. 3D cell culture. Physiology, 32(4), 266-277 (2017).

[2] Carragher, N., Piccinini, F., Tesei, A., Jr, O. J. T., Bickle, M., & Horvath, P. Concerns, challenges and promises of high-content analysis of 3D cellular models. Nature reviews Drug discovery, 17(8), 606-606 (2018).

[3] Sawant-Basak, A., & Obach, R. S. Emerging models of drug metabolism, transporters, and toxicity. Drug Metabolism and Disposition, 46(11), 1556-1561 (2018).

[4] Sant, S., & Johnston, P. A. The production of 3D tumor spheroids for cancer drug discovery. Drug Discovery Today: Technologies, 23, 27-36 (2017).

[5] Vogt, N. Assembloids. Nature Methods, 18(1), 27-27 (2021).

[6] Zanoni, M., Piccinini, F., Arienti, C., Zamagni, A., Santi, S., Polico, R., ... & Tesei, A. 3D tumor spheroid models for in vitro therapeutic screening: a systematic approach to enhance the biological relevance of data obtained. Scientific reports, 6(1), 19103 (2016).

[7] Huang, B. W., & Gao, J. Q. Application of 3D cultured multicellular spheroid tumor models in tumor-targeted drug delivery system research. Journal of controlled release, 270, 246-259 (2018).

[8] LeSavage, B. L., Suhar, R. A., Broguiere, N., Lutolf, M. P., & Heilshorn, S. C. Next-generation cancer organoids. Nature materials, 21(2), 143-159 (2022).

[9] Peirsman, A., Blondeel, E., Ahmed, T., Anckaert, J., Audenaert, D., Boterberg, T., ... & De Wever, O. MISpheroID: a knowledgebase and transparency tool for minimum information in spheroid identity. *Nature methods*, *18*(11), 1294-1303 (2021).

[10] Wang, Y., & Jeon, H. 3D cell cultures toward quantitative high-throughput drug screening. Trends in Pharmacological Sciences, 43(7), 569-581 (2022).

[11] Chen, Z., Ma, N., Sun, X., Li, Q., Zeng, Y., Chen, F., ... & Gu, Z. Automated evaluation of tumor spheroid behavior in 3D culture using deep learning-based recognition. Biomaterials, 272, 120770 (2021).

[12] Akshay, A., Katoch, M., Abedi, M., Shekarchizadeh, N., Besic, M., Burkhard, F. C., ... & Gheinani, A. H. SpheroScan: a user-friendly deep learning tool for spheroid image analysis. GigaScience, 12, giad082 (2023).

[13] Grexa, I., Diosdi, A., Harmati, M., Kriston, A., Moshkov, N., Buzas, K., ... & Horvath, P. SpheroidPicker for automated 3D cell culture manipulation using deep learning. Scientific Reports, 11(1), 14813 (2021).

[14] Swinney, D. C., & Anthony, J. How were new medicines discovered?. Nature reviews Drug discovery, 10(7), 507-519 (2011).

[15] Hötte, K., Koch, M., Hof, L., Tuppi, M., Moreth, T., Verstegen, M. M., ... & Pampaloni, F. Ultra-thin fluorocarbon foils optimise multiscale imaging of three-dimensional native and optically cleared specimens. Scientific Reports, 9(1), 17292 (2019).

[16] Stelzer, E. H., Strobl, F., Chang, B. J., Preusser, F., Preibisch, S., McDole, K., & Fiolka, R. Light sheet fluorescence microscopy. Nature Reviews Methods Primers, 1(1), 73 (2021).

[17] Piccinini, F., Balassa, T., Carbonaro, A., Diosdi, A., Toth, T., Moshkov, N., ... & Horvath, P. Software tools for 3D nuclei segmentation and quantitative analysis in multicellular aggregates. Computational and structural biotechnology journal, 18, 1287-1300 (2020).

[18] de Medeiros, G., Ortiz, R., Strnad, P., Boni, A., Moos, F., Repina, N., ... & Liberali, P. Multiscale light-sheet organoid imaging framework. Nature Communications, 13(1), 4864 (2022).

[19] Piccinini, F., Tesei, A., Zanoni, M., & Bevilacqua, A. ReViMS: Software tool for estimating the volumes of 3-D multicellular spheroids imaged using a light sheet fluorescence microscope. Biotechniques, 63(5), 227-229 (2017).

[20] Mund, A., Coscia, F., Kriston, A., Hollandi, R., Kovács, F., Brunner, A. D., ... & Mann, M. Deep Visual Proteomics defines single-cell identity and heterogeneity. Nature Biotechnology, 40(8), 1231-1240 (2022).

[21] Eisenstein, M. AI under the microscope: the algorithms powering the search for cells. Nature, Nature 623, 1095-1097 (2023).

[22] Piccinini, F., Tesei, A., Arienti, C., & Bevilacqua, A. Cancer multicellular spheroids: volume assessment from a single 2D projection. Computer methods and programs in biomedicine, 118(2), 95-106 (2015).

[23] Diosdi, A., Hirling, D., Kovacs, M., Toth, T., Harmati, M., Koos, K., ... & Horvath, P. A quantitative metric for the comparative evaluation of optical clearing protocols for 3D multicellular spheroids. *Computational and Structural Biotechnology Journal*, *19*, 1233-1243 (2021).

[24] Diosdi, A., Hirling, D., Kovacs, M., Toth, T., Harmati, M., Koos, K., ... & Horvath, P. Cell lines and clearing approaches: a single-cell level 3D light-sheet fluorescence microscopy dataset of multicellular spheroids. Data in Brief, 36, 107090 (2021).

[25] Piccinini, F. AnaSP: a software suite for automatic image analysis of multicellular spheroids. Computer Methods and Programs in Biomedicine, 119(1), 43-52 (2015).

[26] Weigert, M., Schmidt, U., Haase, R., Sugawara, K., & Myers, G. Star-convex polyhedra for 3D object detection and segmentation in microscopy. In Proceedings of the IEEE/CVF winter conference on applications of computer vision, 3666-3673 (2020).

Acknowledgements:

We acknowledge support from the Lendület BIOMAG grant (no. 2018–342), TKP2021-EGA09, Horizon-BIALYMPH, Horizon-SYMMETRY, Horizon-SWEEPICS, H2020-Fair-CHARM, HAS-NAP3, the ELKH-Excellence grant from OTKA-SNN no. 139455/ARRS, the FIMM High Content Imaging and Analysis Unit (FIMM-HCA; HiLIFE-HELMI), and Finnish Cancer Society. F.P. acknowledges support from the MAECI Science and Technology Cooperation Italy-South Korea Grant Years 2023–2025 by the Italian Ministry of Foreign Affairs and International Cooperation (CUP project: J53C23000300003); M.H from the ÚNKP-23-4 -SZTE-639 New National Excellence Program of the Ministry for Culture and Innovation from the source of the National Research, Development and Innovation Fund. The authors would like to thank Lilla Pintér (HUN-REN BRC, Szeged, Hungary) for her technical support.

Funding:

Nothing to declare.

Author contributions:

Conceptualisation: A.D., M.H., F.Pi., P.H.;
Methodology: A.D., T.T., I.G., B.S., M.H.;
Software: F.K., A.K.;
Validation: A.D., T.T., I.G., N.H.;
Formal analysis: A.D., M.H., F.Pi., P.H.;
Investigation: A.D., T.T., I.G., B.S., N.H., F.Pa.;
Resources: A.D., I.G., F.K., A.K., M.H., K.B., F.Pi., P.H.;
Data curation: A.D., T.T., I.G., B.S., M.H.;
Writing-original draft preparation: A.D., M.H., F.Pi.;
Writing-review and editing: T.T., I.G., B.S., N.H., F.K., A.K., K.B., F.Pa., P.H.;
Visualisation: A.D., B.S.;
Supervision: K.B., F.Pa., P.H.;
Project administration: A.D., K.B., F.Pi., P.H.;
Funding acquisition: K.B., F.Pi., P.H.;
All authors read and approved the final version of the manuscript.

Competing interests:

Akos Diosdi and Peter Horvath declare a competing interest as holding a patent related to the technology discussed in the paper (*P2200213*). Akos Diosdi, Ferenc Kovacs, Andras Kriston, and Peter Horvath are employed by Single-cell Technologies Ltd., Szeged, Hungary. The remaining authors declare that the research was conducted in the absence of any commercial or financial relationships that could be construed as a potential conflict of interest.

Data and materials availability:

All data needed to evaluate the conclusions in the paper are present in the paper and/or the Supplementary Materials. Additional data related to this paper may be requested from the corresponding author.

Supplementary Materials:

Supplementary Table 1. Number of publications starting from 2010 to 2023 including different queries based on PubMed.
Query 1: spheroid, organoid, tumoroid.
Query 2: spheroid, organoid, tumoroid, AND confocal, light-sheet, multiphoton, brightfield, bright field, bright-field, phasecontrast, phase contrast, phase-contrast.
Query 3: high content, high-content, high throughput, high-throughput.
Query 4: high content, high-content, high throughput, high-throughput, AND confocal, light-sheet, multiphoton, brightfield, bright field, bright-field, phasecontrast, phase contrast, phase-contrast.
Query5: spheroid, organoid, tumoroid, tumouroid, AND high content, high-content, high throughput, high-throughput, AND confocal, brightfield, bright field, bright-field, phasecontrast, phase contrast, phase-contrast.
Query 6: spheroid, organoid, tumoroid, tumouroid, AND high content, high-content, high throughput, high-throughput, AND confocal, light-sheet, multiphoton, AND 3D.

Year	*Query 1*	*Query 2*	*Query 3*	*Query 4*	*Query 5*	*Query 6*
2010	550	28	12889	154	3	1
2011	637	42	14799	178	2	1
2012	847	46	17104	212	1	1
2013	1065	57	19628	217	1	2
2014	1113	60	21565	233	4	4
2015	1355	79	24058	273	5	3
2016	1702	78	26234	255	6	5
2017	2127	104	27778	286	7	2
2018	2542	107	30107	318	13	9
2018	2947	124	33090	341	9	6
2019	3967	143	37530	339	14	8
2020	4825	156	41056	359	9	7
2021	4753	135	41492	347	21	16
2022	5259	153	39056	368	16	11
SUM	33689	1312	386386	3880	111	76

Supplementary Table 2. Microscope settings used for imaging (Numerical Aperture - NA; Dry - D; Water immersion - W).

#	Microscope	Type	Objectives	NA	Pixel resolution	µm resolution	Coefficient	TwinFlect mirror
1	Leica SP8 TCS	Detection	2.5x	0.07 D	1392 x 1040	3588.78 x 2680.62	2.57783289	-
2	Leica SP8 TCS	Detection	5x	0.15 D	1392 x 1040	1794.39 x 1340.31	1.28891644	-
3	Leica SP8 TCS	Detection	10x	0.32 D	1392 x 1040	897.2 x 670.16	0.64446242	-
4	Leica SP8 TCS	Detection	20x	0.4 D	1392 x 1040	448.6 x 335.08	0.32223121	-
5	Leica SP8 DLS	Detection	10x	0.3 W	2048 x 2048	735.76 x 735.76	0.35925781	5 mm
6	Leica SP8 DLS	Detection	25x	0.95 W	2048 x 2048	294.3 x 294.3	0.14370117	2.5 mm
7	Leica SP8 DLS	Illumination	2.5x	0.07 D	-	-	-	-
8	Leica SP8 DLS	Illumination	5x	0.15 D	-	-	-	-

Supplementary Table 3. Relative differences between the various settings compared to the 20x objective. Spheroids imaged by the Leica SP8 TCS microscope with 2.5x, 5x, 10x, and 20x objectives were used. The 2D morphological characteristics of 50 spheroids were analysed using BIAS and AnaSP then the relative differences compared to the 20x objective were measured for features such as Diameter, Perimeter, Area, Volumetry, Circularity, Sphericity, and Convexity. The average values for each objective were displayed. n=50

#	Features	2.5x objective	5x objective	10x objective
1	Diameter	1.59	1.42	1.15
2	Perimeter	4.15	2.06	1.70
3	Area	2.46	2.29	2.65
4	Volumetry	6.43	5.44	5.48
5	Circularity	3.57	1.32	1.18
6	Sphericity	4.81	1.90	2.10
7	Convexity	3.18	1.70	1.78
	Average	3.74	2.30	2.29

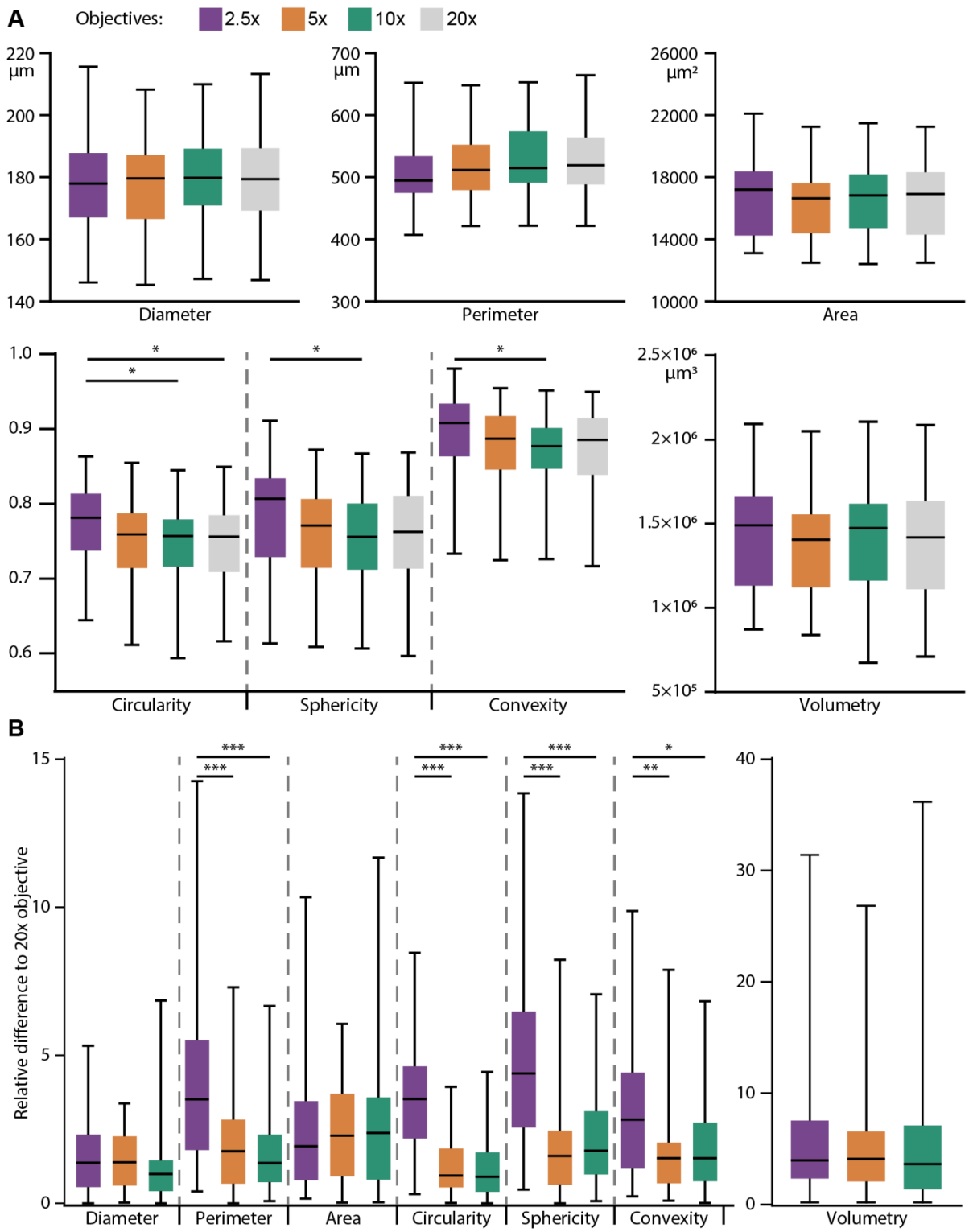

Supplementary Fig.1: Boxplot analysis of various 2D morphological features of 50 spheroids imaged by the Leica SP8 TCS microscope with 2.5x (purple), 5x (orange), 10x (green), and 20x (grey) objectives. Brightfield images of spheroids were manually annotated and 2D morphological features were extracted by using BIAS and AnaSP. (**A**) Boxplot analysis of Diameter (µm), Perimeter (µm), Area (µm^2), Volumetry (µm^3), Circularity (-), Sphericity (-), and Convexity (-). (**B**) Figures represent the relative difference of the same features compared to the 20x objective. Each statistical test was carried out by features separately. n=50; *p ≤ 0.05; **p ≤ 0.01; ***p ≤ 0.001.

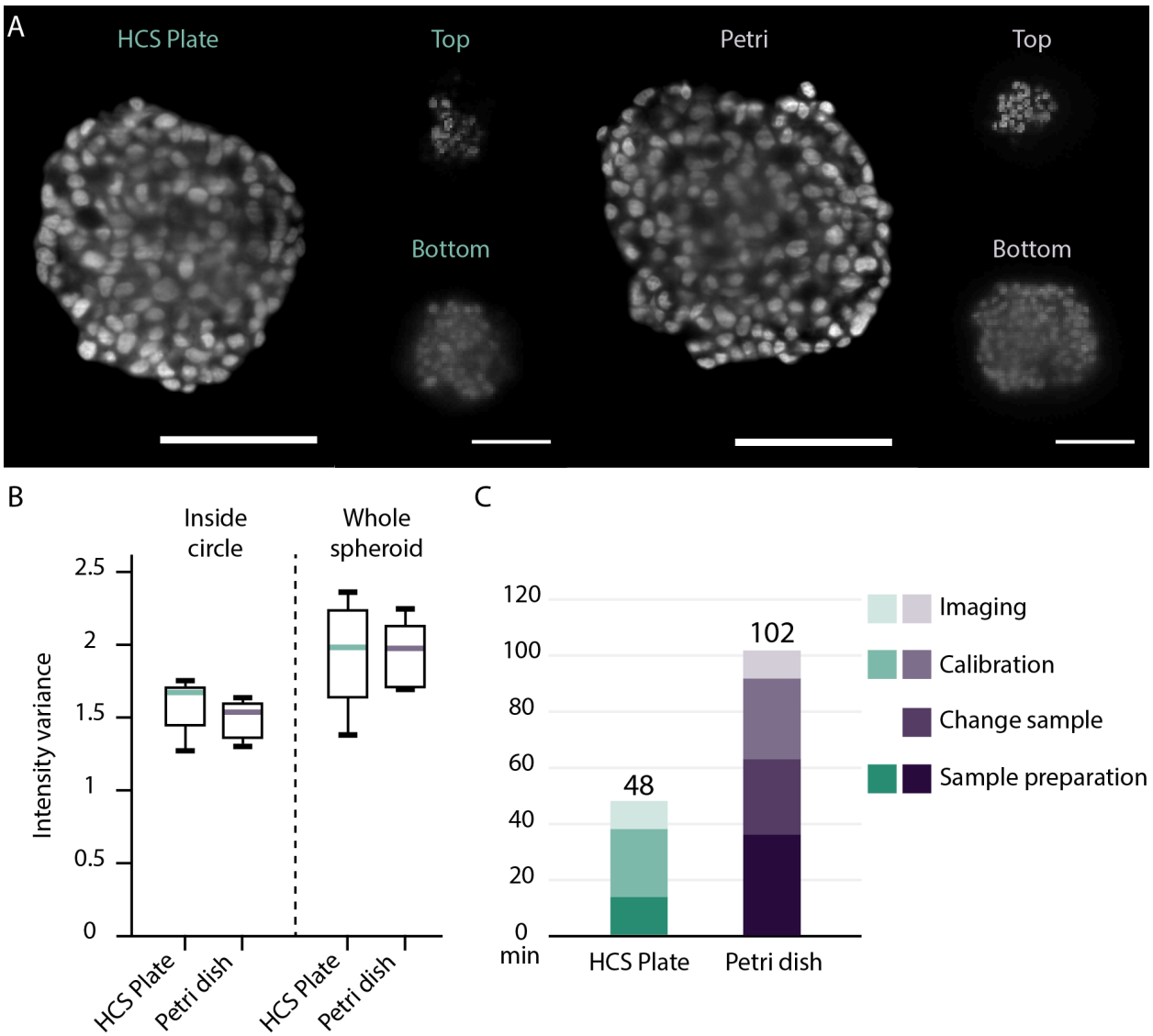

Supplementary Fig.2 Qualitative comparison of the HCS plate and the traditional imaging method where the samples were placed into Petri dishes. (**A**) Fluorescent images of T-47D spheroids stained with DRAQ5 were used as a reference to compare image quality. Randomly selected spheroids screened in the HCS plate (left image) and in Petri dish (right image) were visualized where images were selected from the top, middle, and bottom regions. Scale bars represent 100 µm. (**B**) To characterise the general blurriness of the whole z-stack, the Intensity variance metric was used both for the inside circle and for the whole spheroid. Results were shown in a boxplot figure where no significant differences were measured. n=5 for each group. (**C**) Preparation and screening times were measured for both techniques and 4 sections were distinguished. Starting from the darkest volume the 4 categories are Sample preparation, Change sample (this category does not apply to the HCS plate), Calibration, and Imaging. The total time was calculated for 10 samples for each method.

Supplementary Note 1:

HCS PLATE COMPONENTS

FEP foil

Fluorinated Ethylene Propylene (FEP) foils are transparent, with a refractive index of 1.341-1.347. FEP is chemically inert and resistant to most organic solvents, acids, and bases. Additionally, the material satisfies FDA (21CFR.177.1550) and EU (2002/72/EC) requirements (Hötte, K., *et al.*, Scientific Reports, 2019). FEP-films (Holscot Europe, Netherlands) with a 50 µm thickness were cut into 15x15 cm pieces and cleaned with 70% alcohol. Each foil was placed and clamped into the frame of a JT-18 vacuum-forming machine (Yuyao Jintai Machine Company, China). To get small and uniform shapes, the heater needs to raise the temperature to a level near the glass transition temperature of the FEP-foil which is between 260-280°C. Once the heater reaches the desired temperature, the positive mould is quickly placed onto the vacuum-forming machine, and the foil is quickly pressed onto the mould while the vacuum suction is switched on. The FEP foil that has been extruded is then carefully taken out of the mould and cleaned with an isopropyl alcohol bath for 5 min to remove the excess resin components. A 3D-printed holder was designed to provide support for the foil while transferring samples.

Insert element

To fix the samples' position inside the cuvettes, hydrogels or a 3D-printed insert element are suitable (**Supplementary Note 1 Fig.1a)**. While hydrogels are optimal for smaller samples, the insert element offers an alternative solution to secure the position within the foil. The insert element contains the same pyramid-like structure as the foil, however, there is no sphere at the top. Inserting the element inside the cuvettes secures all samples in the spheres without deforming or harming the cells. To elevate the samples from the bottom to the same z-positions, the FEP foil with hydrogel or insert element should be turned over and placed inside of the base element. To provide precise positioning and a locking mechanism of the cuvettes inside of the base, the insert contains 4 magnets that attach to the 4 other magnets on the base.

Base element

The base components of the plate were printed with the Prusa i3 MK3S+ 3D printer with PETG (3DP-PETG1.75-01-BK; Gembird, Shenzhen, China) in two different size versions (**Supplementary Note 1 Fig.1b)** with the corresponding grid elements (**Supplementary Note 1 Fig.1c** and **d)**. The bigger version is 85 mm / 127 mm / 15.4 mm (average size of a 96-well plate) which is suitable for screening 56 samples, while the smaller version 85 mm / 73.8 mm / 15.4 mm was designed only for 28 samples. To create a waterproof base for the samples, the 24 mm / 64 mm coverslips (Menzel Gläser, Germany) were secured with silicone grease (ThermoFisher, USA) to the bottom of the bases. Models were designed in Blender and STL files (stereolithography files) were exported to *PrusaSlicer v 2.6.x*. All models were 3D printed with the default Prusa PETG filament profile and with "0.4 Quality print settings" using a 0.4 nozzle.

Grid element

To secure the foil's position in the plate we printed a secure element that allows to fix the position of the FEP foil within the base (**Supplementary Note 1 Fig.1c** and **d)**. This compartment was printed with the Prusa i3 MK3S+ printer.

Positive mould

A positive mould for the spikes was created using *Blender 3.0*. Each mould was designed to fit perfectly into the base of the plate (**Supplementary Note 1 Fig.2a)**. For printing, the 3D models were exported to a stereolithographic file format (.stl) and then imported into *PrusaSlicer v 2.6.x* (Prusa Research, Czech Republic). Each heat-resistant mould was printed with the Prusa SL1 printer, which is a stereolithography (SLA) resin-based 3D printer that forms objects layer by layer using a liquid resin that is UV-cured. For printing, the DruckWege Type D High Temp resin (TDH-VIO-500, Groningen, The Netherlands) was used. This printer provides high-resolution printing capabilities enabling the production of intricate and detailed objects with smooth surface finishes. The mechanical and thermal characteristics of heat-resistant resin enable it to endure the vacuum-forming process. The positive moulds are UV-cured and washed with isopropanol to remove excess resin from the surface. Then the moulds were examined under a stereomicroscope and cleaned by submerging them in an ultrasonic bath before being used.

ASSEMBLY OF THE HCS PLATE

First, biological samples should be placed precisely into the cuvettes of the FEP foil. An additional 3D printed element which is not part of the HCS plate can be used to prevent the movement of the foil while transferring the samples (***Supplementary Note 1***

Fig.2c). Prefilling with liquid the cuvettes of the foil before sample transfer can help remove air bubbles. The sample transferring process can be done manually, using a single or multi-channel pipette (8 channels) or a pipetting robot. After pipetting, a visual check is necessary because all the samples should sink to the bottom of the cuvette and positioned in the middle. If a sample is not in the middle of the cuvette, a gentle shake of the foil or pipetting the samples to the bottom may resolve this issue. If all the samples reach the bottom of the cuvettes of the FEP foil and there are no air bubbles next to the samples, then the position of the samples should be secured. Removing the excess mounting media from the cuvettes allows to pipette a low melting point agarose to fix the position of the 3D sample inside the foil. The alternative solution is to gently push the insert element into the FEP foil until each cuvette is secured. By utilising either method, samples should be ready to be placed into the base element, by turning over the whole FEP foil containing all the samples. At this point, all the samples should be at the top of the cuvettes covered by the transparent foil. Next, the FEP foil with the samples should be placed into the base element, where each cuvette is positioned within the coverslip. After checking the alignment of the cuvettes, the user must carefully fill the plate with the detection solution by removing all the air bubbles under the FEP foil. Before filling up completely, the grid element should be placed on top of the FEP foil to stabilise and prevent additional movements of the samples. Finally, before inserting the base into the microscope, the plate with the detection solution must be carefully filled to proceed with the calibration process (**Supplementary Note 1 Fig.2b**).

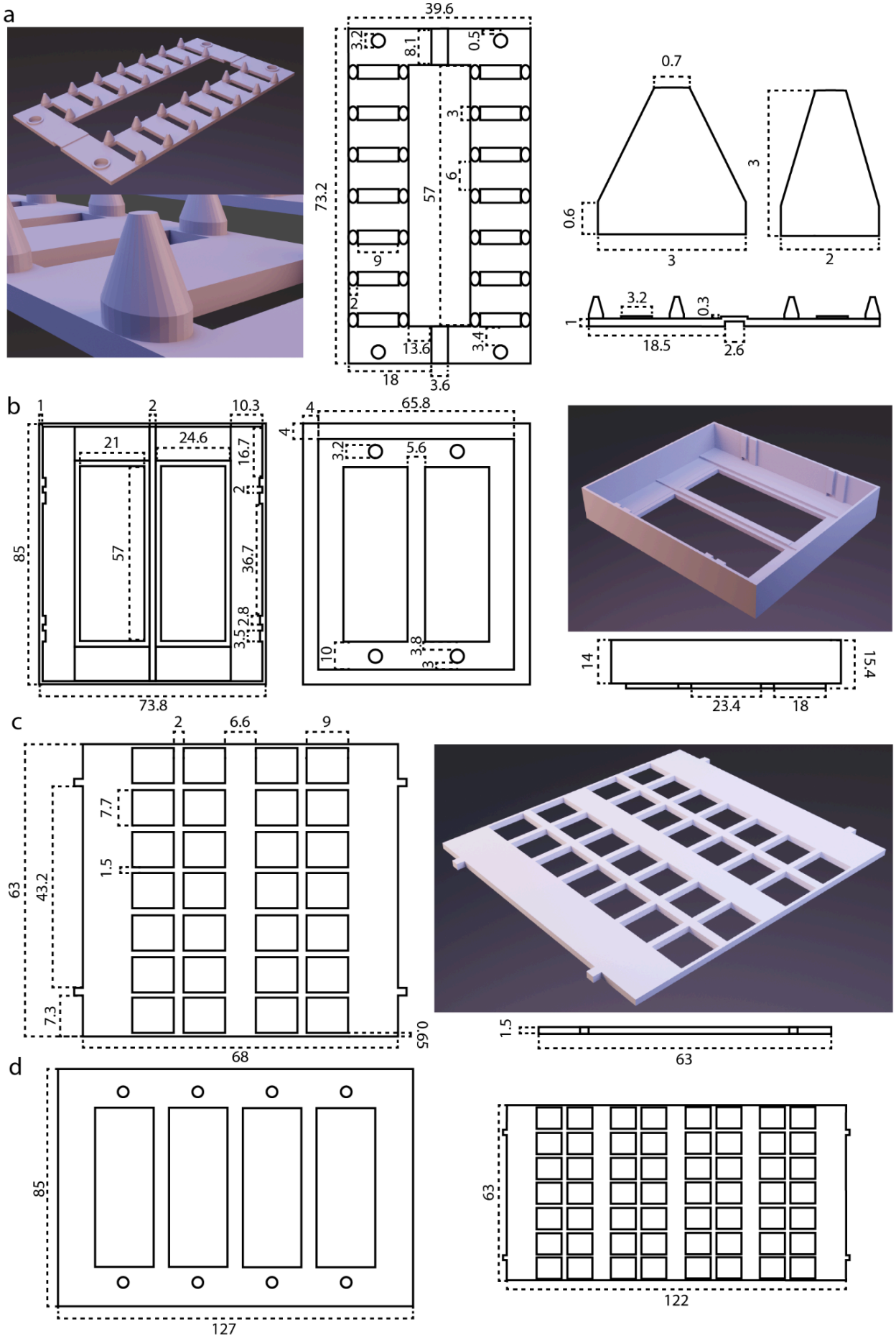
a
39.6
3.2
8.1
0.5
3
6
73.2
57
9
2
13.6
3.4
18
3.6
0.7
3
0.6
3
2
3.2
0.3
1
18.5
2.6
b
1
2
10.3
21
24.6
16.7
2
85
57
36.7
2.8
3.5
73.8
4
65.8
4
3.2
5.6
10
3.8
3
14
15.4
23.4
18
c
2
6.6
9
7.7
1.5
63
43.2
7.3
0.65
68
1.5
63
d
85
127
63
122

Supplementary Note 1 Fig.1. **HCS Plate 3D printed elements (first part).** (**a**) The smaller version of the base element is designed for 28 samples within one plate. (**b**) Prusa SL1 stereolithography (SLA) resin-based 3D printer was used to 3D print the insert element that secures the position of the samples within the vacuum-formed FEP foil. (**c**) Grid element that can be placed into the base element to fix the position of the FEP foil within the plate. (**d**) 3D rendered images representing the fully assembled plate without the FEP foil and the samples for the smaller (28 samples/plate) and the bigger version (56 samples/plate). Blender 3.0 software was used to create each rendered image. The dimensions of the figures are all displayed in millimetres. Every element was printed using a Prusa i3 MK3S+ printer except in cases where it is stated otherwise.

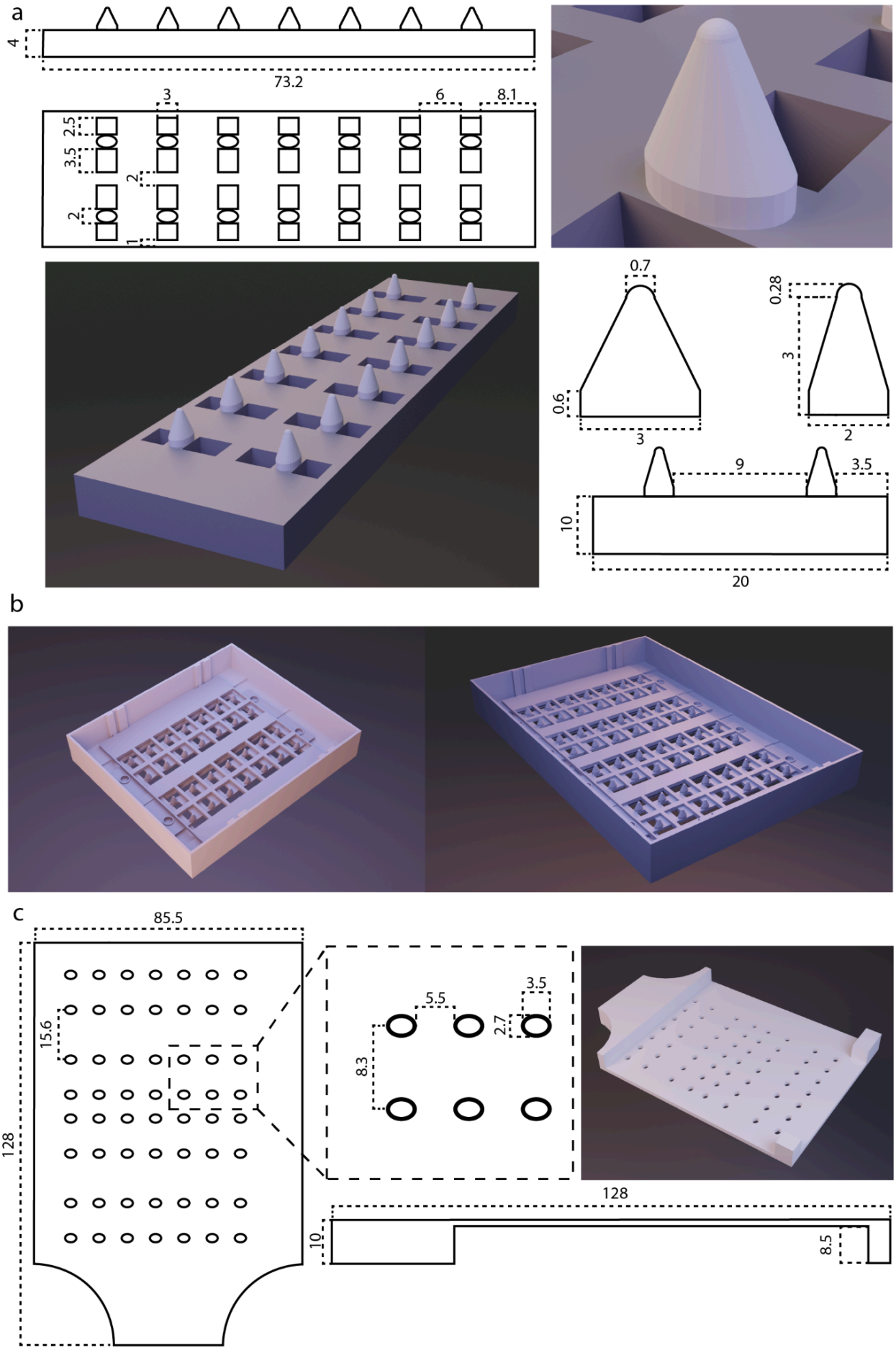
a
4
73.2
3
6
8.1
2.5
3.5
2
2
1
0.7
0.6
3
0.28
3
2
9
3.5
10
20
b
c
85.5
15.6
128
5.5
3.5
2.7
8.3
128
10
8.5

Supplementary Note 1 Fig.2. **HCS Plate 3D printed elements (second part)**. (**a**) Positive mould element used for vacuum-forming, printed with the Prusa SL1 SLA resin-based 3D printer. (**b**) 3D printed base element that is made for 56 samples where all dimensions are identical to the smaller version except for the highlighted values. On the right side, the modified version of the grid element is shown that can be placed into the bigger base element. (**c**) An additional 3D printed element was made to prevent the moving of the vacuum-formed FEP foil while samples are transferred into the foil. This element is not part of the HCS plate and it is not needed for the assembly. *Blender 3.0* software was used to create each rendered image. The dimensions of the figures are all displayed in millimetres. Every element was printed using a Prusa i3 MK3S+ printer except in cases where it is stated otherwise.